Research Article

Huanran Lin, Xiuhua Guo*, Kexing Song*, Jiang Feng, Shaolin Li, and Xiangfeng Zhang

Synergistic strengthening mechanism of copper matrix composite reinforced with nano-Al_2O_3 particles and micro-SiC whiskers

https://doi.org/10.1515/ntrev-2021-0006
received January 22, 2021; accepted February 5, 2021

Abstract: Although Cu–Al_2O_3 composites have good comprehensive performance, higher mechanical properties and arc erosion resistance are still required to meet heavy-duty applications such as electromagnetic railguns. In this work, a novel hybrid SiC_w/Cu–Al_2O_3 composite was successfully prepared by combining powder metallurgy and internal oxidation. The microstructure and mechanical behavior of the SiC_w/Cu–Al_2O_3 composite were studied. The results show that nano-Al_2O_3 particles and micro-SiC_w are introduced into the copper matrix simultaneously. Well-bonded interfaces between copper matrix and Al_2O_3 particles or SiC_w are obtained with improved mechanical and arc erosion resistance of SiC_w/Cu–Al_2O_3 composite. The ultimate tensile strength of the SiC_w/Cu–Al_2O_3 composite is 508.9 MPa, which is 7.9 and 56.1% higher than that of the Cu–Al_2O_3 composite and SiC_w/Cu composite, respectively. The strengthening mechanism calculation shows that Orowan strengthening is the main strengthening mechanism of the SiC_w/Cu–Al_2O_3 composite. Compared with Cu–Al_2O_3 composite, the hybrid SiC_w/Cu–Al_2O_3 composite has lower arc time and energy and better arc stability.

Keywords: SiC whiskers, nano-Al_2O_3 particles, SiC_w/Cu–Al_2O_3 composite, mechanical properties, synergistic strengthening effect

1 Introduction

Cu–Al_2O_3 composites have a wide range of applications in electrical contact due to their excellent conductivity [1] and high strength at elevated temperatures. For example, in the electromagnetic railguns system, the guide rail is seriously worn and partly melted due to the high projectile launching speed and driving current of the armature/guide rail system [2]. This kind of equipment puts forward higher requirements on mechanical properties [3], current-carrying friction and wear resistance, and arc erosion resistance of materials [4]. However, the commercial Cu–Al_2O_3 composites cannot meet the above requirements, and copper matrix materials used in the guide rail with better mechanical and electrical erosion resistance are still not developed.

Recently, hybrid copper matrix composites with two or more reinforcing phases have present better performance compared with the copper matrix composites reinforced by a single reinforcement [5]. And, the reported papers on synergistic reinforcements are mainly focused on CNTs [6]; Cr [7] and WC particles [8] strengthened the Cu–Al_2O_3 composite [9]. For example, Zhang *et al.* [10] reported that the ultimate tensile strength of a Cu–Al_2O_3–La composite was 309 MPa. Pan *et al.* [11] found that the ultimate tensile strength (345 MPa) of Cu–6.1 vol% CNTs–1.2 vol% Al_2O_3 composite was 41.1% higher than that of Cu-CNTs composite. Singh and Gautam [12]

* **Corresponding author: Xiuhua Guo,** School of Materials Science and Engineering, Henan University of Science and Technology, Luoyang, China; Key Laboratory of Materials Science & Processing Technology for Non-ferrous Metals of Henan, Luoyang, China; Provincial and Ministerial Co-construction of Collaborative Innovation Center for Non-ferrous Metal New Materials and Advanced Processing Technology, Luoyang, China, e-mail: guoxiuhua@haust.edu.cn
* **Corresponding author: Kexing Song,** School of Materials Science and Engineering, Henan University of Science and Technology, Luoyang, China; Key Laboratory of Materials Science & Processing Technology for Non-ferrous Metals of Henan, Luoyang, China; Provincial and Ministerial Co-construction of Collaborative Innovation Center for Non-ferrous Metal New Materials and Advanced Processing Technology, Luoyang, China, e-mail: kxsong@haust.edu.cn
Huanran Lin, Jiang Feng, Shaolin Li, Xiangfeng Zhang: School of Materials Science and Engineering, Henan University of Science and Technology, Luoyang, China; Key Laboratory of Materials Science & Processing Technology for Non-ferrous Metals of Henan, Luoyang, China; Provincial and Ministerial Co-construction of Collaborative Innovation Center for Non-ferrous Metal New Materials and Advanced Processing Technology, Luoyang, China

discovered that the ultimate tensile strength of Cu–0.5 vol% WC–5.0 vol% Al_2O_3-2.4 vol% Cr composite (385 MPa) was 71.9% higher than that of pure copper (224 MPa). Although the addition of particles or whiskers is beneficial to improve the mechanical properties of Cu–Al_2O_3 composites, their ultimate tensile strength are still under 400 MPa [13]. The reason for the low mechanical property is the poor interface bonding between reinforcements and copper matrix, in which the reinforced phases are introduced into the copper matrix by a common powder metallurgy process [14]. However, hybrid copper-based materials with high mechanical properties fabricated by in-situ synthesis have not yet been reported.

Currently, SiC_w has become a potential reinforcement phase in copper-based materials, which has the advantages of low density [15], high strength [16], corrosion resistance [17], and high-temperature stability [18]. The object of this work is to develop a novel SiC_w/Cu–Al_2O_3 composite with well-bonded interfaces between copper matrix and reinforcements. And, the preparation procedure combined powder metallurgy and internal oxidation, and the nano-Al_2O_3 particles and micro-SiC_w were introduced into the copper matrix simultaneously. The well-bonded interfaces between copper matrix and Al_2O_3 particles or SiC_w are obtained with improved mechanical and arc erosion resistance. The strengthening mechanisms of the SiC_w/Cu–Al_2O_3 composite were calculated and discussed. The fabrication procedures and experimental results can provide a reference for the design and preparation of high-performance copper matrix composites.

2 Experiment

2.1 Materials and methods

The raw materials used in the preparation of composites are Cu–0.2 wt% Al alloy powders (99.6% purity, the median particle size of 40 μm, Hunan Huabang Powder Material Co., Ltd), Cu_2O powders (provide oxygen for internal oxidation, 99.8% purity, the median particle size of 1 μm, Shanghai Xiangtian Nano Materials Co., Ltd), and SiC whiskers (98% purity, 5–10 μm length and 0.5 μm diameter).

The experimental procedures were as follows: first, mixing of powders was performed. Cu–0.2 wt% Al alloy powder, Cu_2O powder, and SiC_w were mixed in appropriate proportions. The powders were blended by a QQM/B light ball mill for 16 h at 35 rpm and a ball-to-powder ratio of 5:1. Note that to realize the complete internal oxidation of Al to produce Al_2O_3 in the subsequent internal oxidation process, the mass ratio of Cu_2O powder to Cu_2O powder is calculated to be 1.1:1 [19] (M(Cu–0.2 wt% Al):M(Cu_2O) = 56.8:1). Second, cold isostatic pressing was performed. The mixed powders were pressed into cylindrical samples (Φ50 × 40 mm) in LDJ200/600-300 cold isostatic press at a pressure of 210 MPa and held for 10 min. Third, sintering was performed. The obtained cylindrical samples were sintered in a tube furnace protected by argon at 950°C for 3 h. (Nano-Al_2O_3 particles were formed in the chemical reaction of internal oxidation, and the specific process has been reported in ref. [20]). Finally, the sintered samples were put into a ZT-200-22Y vacuum sintering furnace under a hydrogen–argon atmosphere and kept at 900°C for 2 h for reduction. To further improve the relative density of the copper matrix composites, the sintered samples were put into a YA32-315 four-column hydraulic press for hot extrusion, the extrusion ratio was 10:1, and bars with a diameter of 15 mm were obtained. For comparison, the Cu–Al_2O_3 composite, the SiC_w/Cu composite, and the pure copper were prepared under the same conditions. The specific composition is listed in Table 1.

2.2 Material characterization

The microstructures of composites were observed by inverted metallurgical microscopy (DMi8C, Leica Microsystems Inc). The transmission electron microscopy (TEM) samples were polished by a precision polishing system (GATAN691, USA), and the interface between the matrix and reinforcing phase was characterized by high-resolution transmission electron microscopy (HR-TEM; JEM-2100, JEOL, Japan). The grain size of the copper matrix composites was analyzed by field-emission scanning electron microscopy (FE-SEM; JSM-7800F, JEOL, Japan).

2.3 Performance tests

To evaluate the tensile strength of the composites, the samples were processed into rod-shaped tensile samples with a diameter of 5 mm and a gauge length of 25 mm.

Table 1: Composition of copper matrix composites (vol%)

Materials	Cu	Al_2O_3	SiC_w
Cu	100	—	—
SiC_w/Cu	95.3	—	4.7
Cu–Al_2O_3	99.1	0.9	—
SiC_w/Cu–Al_2O_3	94.4	0.9	4.7

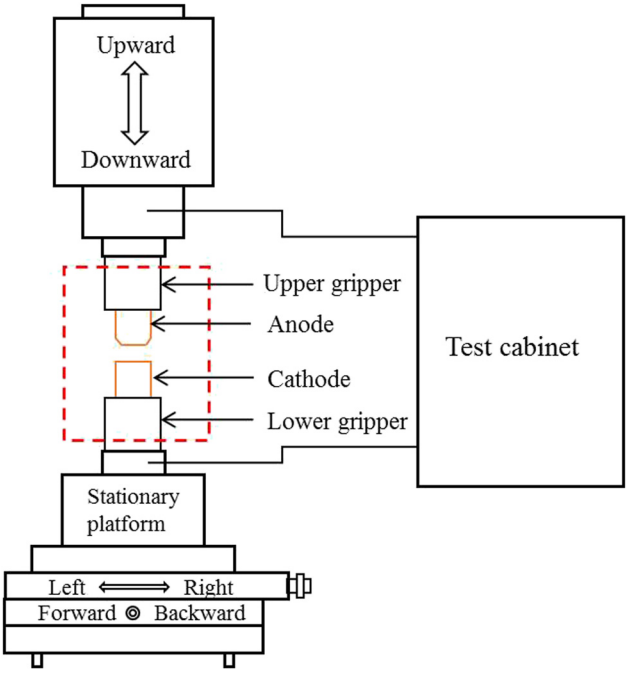

Figure 1: Schematic of JF04C electrical contact test apparatus.

The tensile tests were performed by a tensile testing machine (AUTOGRAPH AG-I 250KN, Japan) by stretching along the extrusion direction with a tensile strain rate of 0.5 mm/min. Tensile fractures were analyzed by scanning electron microscopy (SEM; JSM-IT100, JEOL, Japan).

Electrical contact tests were carried out by an electrical contact tester (JF04C, Kunming Institute of Precious Metals, China) shown in Figure 1. As-extruded samples were processed into electrical contact samples with a diameter of 3.8 mm and a length of 10 mm. Each contact pair was tested for 5,000 operation times under resistance load, with a voltage of 24 V DC, a current of 15 A, an average contact force of 50 cN, and an electrode spacing of 2 mm. Data on arc energy and arcing duration were automatically recorded by the JF04C test system. The arc erosion morphologies of the cathode and anode contacts were observed by SEM (JSM-IT100, JEOL, Japan).

3 Experimental results and discussion

3.1 The microstructure of the $SiC_w/Cu–Al_2O_3$ composite

The metallographic structures of pure copper, the $Cu–Al_2O_3$ composite, and the $SiC_w/Cu–Al_2O_3$ composite are presented in Figure 2. Comparing Figure 2a with Figure 2b shows that the grain size of the $Cu–Al_2O_3$ composite is smaller than that of pure copper, which indicates that Al_2O_3 particles are formed in the process of internal oxidation and can inhibit grain growth. Figure 2b and c show that compared with the $Cu–Al_2O_3$ composite, the grain size of the $SiC_w/Cu–Al_2O_3$ composite has no obvious decrease, which indicates that the addition of SiC_w has a certain influence on the grain size change but has little effect. Figure 2d shows that the SiC whiskers are arranged in an orderly manner and distributed along the extrusion direction without large-area agglomeration.

Figure 3 shows the high-resolution transmission electron microscopy (HR-TEM) images of the $SiC_w/Cu–Al_2O_3$ composite. Figure 3a shows that γ-Al_2O_3 particles with a particle size of 3–8 nm are uniformly dispersed in the copper matrix, with an average particle spacing of 50 nm. Fine nano-Al_2O_3 particles are more conducive to pinning dislocations, hindering dislocation movement and grain boundary slip and thus improving the strength of composites [21]. Figure 3b is an Inverse Fast Fourier Transform (IFFT) image of the area in the yellow dotted box in Figure 3a. The interface between γ-Al_2O_3 and the copper matrix is flat, and there are no physical gaps at the interface and no compounds produced by adverse reactions. The HR-TEM image of the interface between SiC_w and the copper matrix in Figure 3d shows that there is an obvious amorphous transition layer at the interface between the copper matrix and SiC_w. This is because Si atoms in SiC diffuse into the copper matrix, leaving only a layer of carbon at the interface between the copper matrix and SiC_w [22]. This can also be proven by the existence of an amorphous diffuse scattering halo in the FFT diagram in the lower-left corner of Figure 3d. Meanwhile, the SAD pattern in the upper right corner Figure 3d shows the SiC diffraction spots, proving that the whiskers used are β-SiC. Compared with α-SiC, β-SiC has better hardness, tensile strength, elastic modulus, and high-temperature resistance, which is more conducive to improve the tensile strength of composites [23]. It is generally believed that the rough or bamboo-like surface of whiskers can increase the friction between whiskers and the matrix, thus improving the interfacial bonding strength [24]. Excessive interfacial strength leads to the fracture of whiskers and copper matrix composites during stretching, which limits the contribution of the whisker pull-out effect to the toughness of copper matrix composites [25]. The amorphous ribbon transition layer formed at the interface between the copper matrix and SiC_w can reduce the interfacial bonding strength, reduce the shear stress that needs to be overcome when whiskers are pulled out,

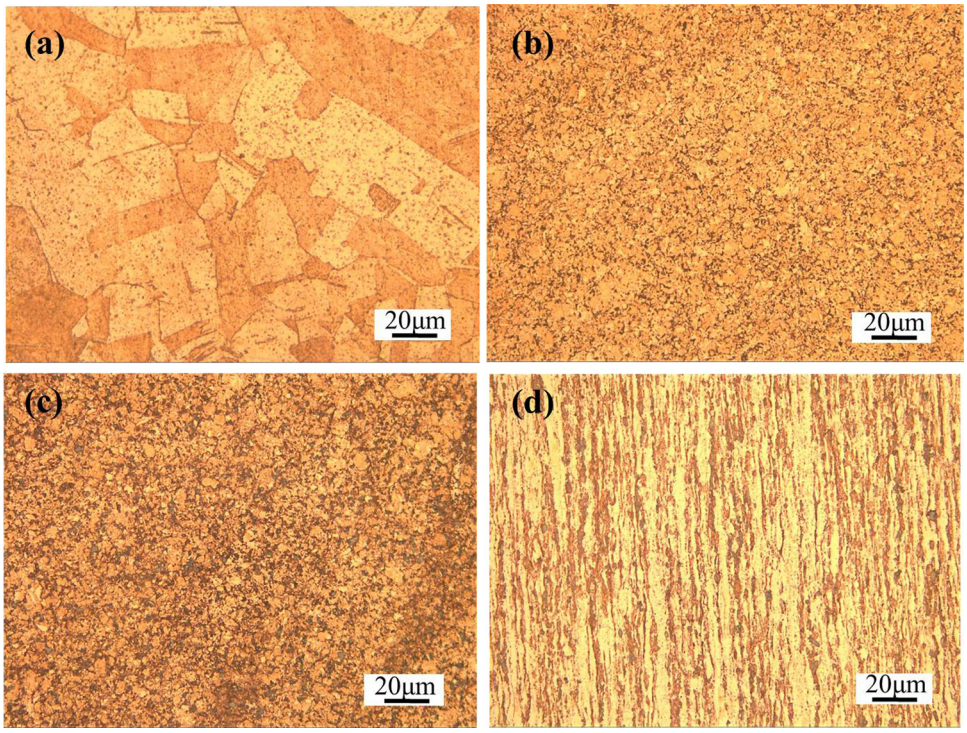

Figure 2: Microstructure of pure copper and its composites: (a) pure copper, (b) Cu–Al_2O_3, (c) cross-sectional microstructure of SiC_w/Cu–Al_2O_3, and (d) longitudinal-section microstructure of SiC_w/Cu–Al_2O_3.

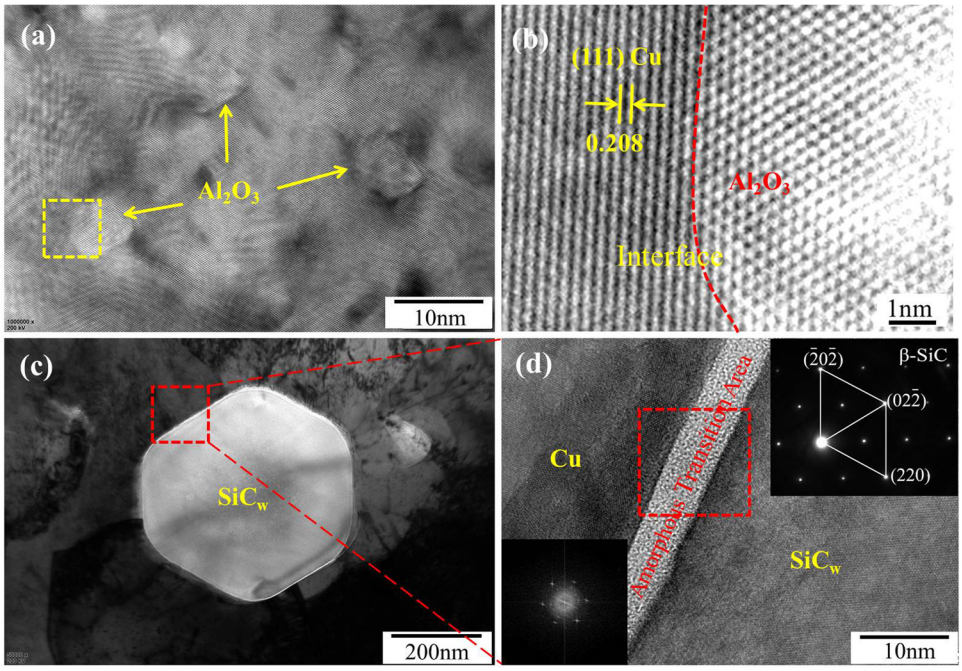

Figure 3: TEM images of the SiC_w/Cu–Al_2O_3 composite: (a) HR-TEM image of nano-Al_2O_3 particles, (b) IFFT image of the boxed area in (a), (c) TEM cross-sectional image of SiC_w, and (d) HR-TEM image of the boxed area in (c).

facilitate whisker pulling out, and play an obvious role in improving the tensile strength and toughness of the composite [26].

3.2 Mechanical properties and fracture morphology of the $SiC_w/Cu–Al_2O_3$ composite

Figure 4 shows the engineering tensile stress–strain curves of pure copper and its composites. In summary, compared with pure copper, the strength of the SiC_w/Cu composite is not greatly improved by adding a single reinforcing phase of SiC_w, but the tensile strength of the $SiC_w/Cu–Al_2O_3$ composite is greatly improved. The addition of the reinforcing phase inevitably led to a decrease in the ductility of the composites [27]. The ultimate tensile strength of pure copper is 228.4 MPa, and the elongation is 50.4%. The ultimate tensile strength of the $Cu–Al_2O_3$ composite is 471.5 MPa, and the elongation is 15.4%. The elongation of the $Cu–Al_2O_3$ composite decreased due to uncoordinated deformation between hard Al_2O_3 particles and the copper matrix, with good plasticity during deformation, which indicated that the tensile strength of the composites increased at the expense of elongation [28]. The ultimate tensile strength of the SiC_w/Cu composite is 246.5 MPa, which is not greatly improved compared with that of pure copper, and its elongation is poor, which may be caused by SiC_w agglomeration. The ultimate tensile strength of the $SiC_w/Cu–Al_2O_3$ composite is 508.9 MPa, and the elongation is 8.5%. Compared with that of the $Cu–Al_2O_3$ and SiC_w/Cu composites, the tensile strength of the $SiC_w/Cu–Al_2O_3$ composite is increased by 7.9 and 51.6%, respectively. The further improvement in tensile strength indicates that the effect of the hybrid reinforcement of SiC_w and nano-Al_2O_3 particles is better than that of the composite reinforced by SiC_w or nano-Al_2O_3 particles alone. Hybrid reinforcement can improve the spatial configuration of each reinforcing phase, which is beneficial to fully exploiting the advantages of SiC_w and nano-Al_2O_3 particles and then improve the strength of copper matrix composites [29].

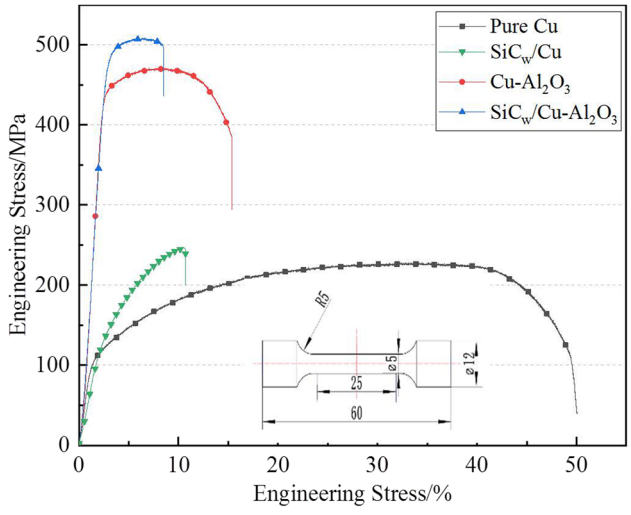

Figure 4: Engineering tensile stress–strain curves of pure copper and composites.

Figure 5 shows the tensile fracture morphology of pure copper and copper matrix composites. The pure copper sample has obvious plastic deformation before fracture, the fracture surface is mainly composed of large and deep dimples and torn edges, and the fracture surface is characterized by a typical micropore aggregation fracture surface, as shown in Figure 5a. Compared with the fracture morphology of pure copper, the dimples of the $Cu–Al_2O_3$ composite become smaller and shallower, which worsens the plasticity of the composite (Figure 5b). Figure 5c shows the fracture morphology of the SiC_w/Cu composite, and there is a large amount of agglomerated SiC_w at the fracture. Agglomerated SiC_w cannot effectively contact the copper matrix, which reduces the interfacial bonding strength and makes it easier to fall off under the action of an external force, resulting in the lower strength of the SiC_w/Cu composite [30]. The fracture morphology of the $SiC_w/Cu–Al_2O_3$ composite (Figure 5d) shows that the axial direction of SiC_w is the same as the tensile direction, which hinders grain boundary slip, and there are "SiC_w bridges" and SiC_w pulling out at the crack. The bridging effect of SiC_w can hinder crack propagation and promote crack deflection. Nano-Al_2O_3 particles can inhibit grain growth and promote crack deflection, which is conducive to improve the strength of composites, and dispersed nano-Al_2O_3 particles are beneficial to improve the plasticity of materials [31].

3.3 Analysis of strengthening mechanism of the $SiC_w/Cu–Al_2O_3$ composite

There are many strengthening mechanisms in composites, such as grain refinement (GR) [32], Orowan strengthening (OS) [33], load transfer (LT) [34], and thermal

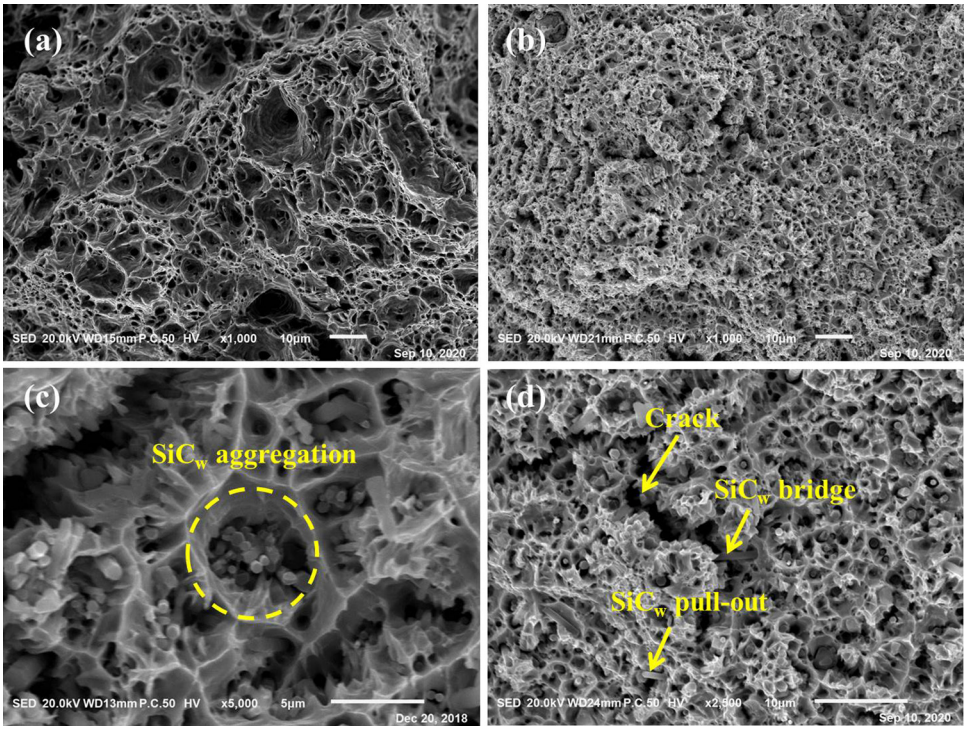

Figure 5: Tensile fracture morphology of copper matrix composites: (a) Pure copper, (b) Cu–Al_2O_3, (c) SiC_w/Cu, and (d) SiC_w/Cu–Al_2O_3.

mismatch (TM) [35]. Due to the different thermal expansion coefficients of the reinforcing phase and copper matrix, thermal mismatch strengthening occurs in the cooling process of the composite material, but the samples will play a considerable role in thermal mismatch strengthening only during rapid cooling [36]. As the cooling process of this test is furnace cooling or slow cooling, the contribution of thermal mismatch strengthening to the strength of materials is temporarily ignored. Therefore, the strength contribution of the SiC_w/Cu–Al_2O_3 composite mainly comes from grain refinement, Orowan strengthening, and load transfer strengthening.

3.3.1 Orowan strengthening

Research shows that long whiskers with large aspect ratios cannot be effectively surrounded by dislocation loops [37]. Therefore, the contribution of Orowan strengthening to the strength of the SiC_w/Cu–Al_2O_3 composite mainly comes from dispersed nano-Al_2O_3 particles. Dislocation lines cannot cut through hard Al_2O_3 particles directly, but bend gradually under the action of external stress until the dislocation lines at both ends meet to form a closed dislocation loop, and the remaining dislocation lines continue to move forward under the action of external force. The Orowan strengthening equation is as follows [38]:

$$\sigma_{OS} = \frac{0.4Gb}{\pi\sqrt{1-\nu}}\frac{1}{L}\ln\left(\frac{D}{b}\right) \tag{1}$$

where G is the shear modulus (42.1 GPa for Cu [39]), ν is the Poisson's ratio (0.326 for Cu [39]), b is the Burger's vector (0.256 nm for Cu [39]), L is the particle spacing, and D is the average particle size. According to the calculation, the contribution of the Orowan strengthening mechanism to the strength of the SiC_w/Cu–Al_2O_3 composite is 145.2 MPa. Equation (1) shows that the smaller the distance between particles is the greater the critical shear stress required for dislocation motion. Dislocation loops around particles also hinder the movement of dislocation sources and other dislocations, and further strengthen the copper matrix.

3.3.2 Grain refinement

Figure 2b and c show that the addition of SiC_w and nano-Al_2O_3 particles can obviously refine the grains. Theoretically, SiC_w also hinders the movement of grain boundaries, but in this experiment, the addition of silicon carbide whiskers has little effect on grain size, and nano-

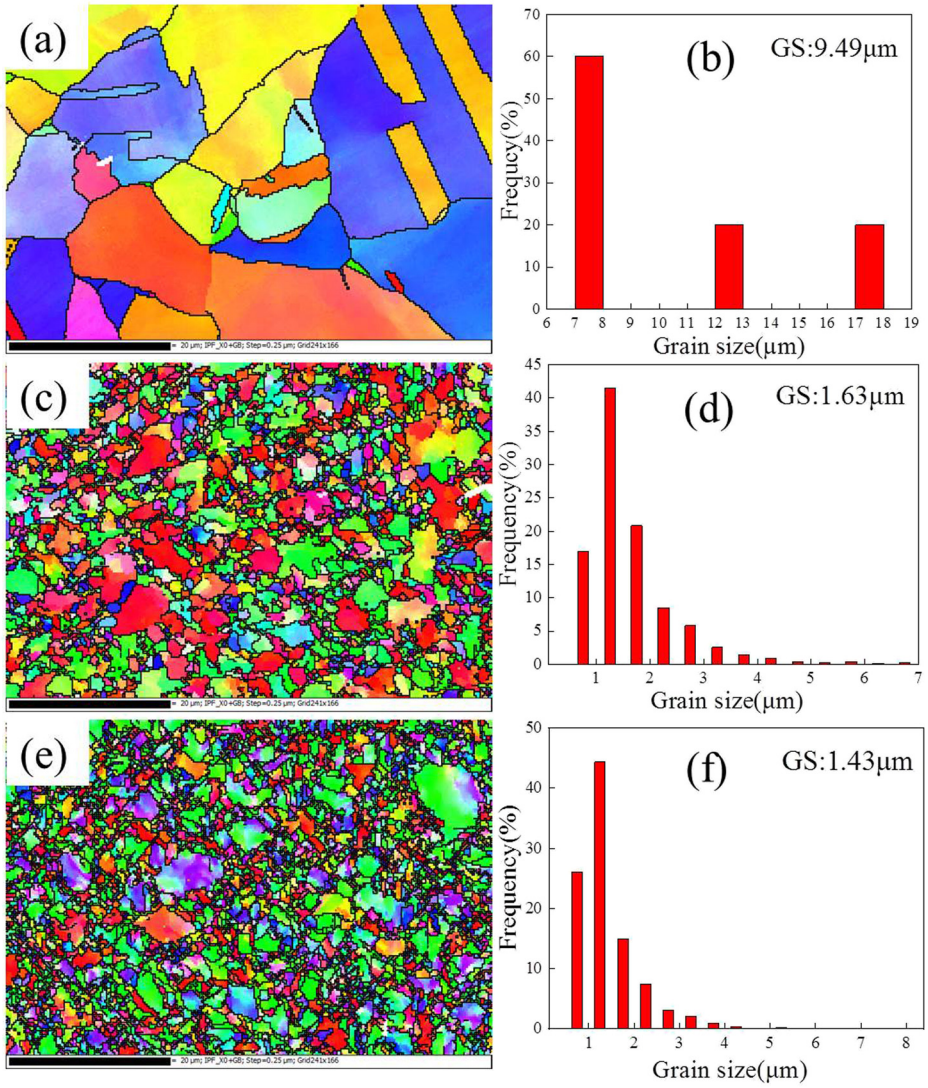

Figure 6: EBSD map (IPF) and grain size distributions of copper matrix composites: (a and b) pure Cu, (c and d) Cu–Al_2O_3, and (e and f) SiC_w/Cu–Al_2O_3.

Al_2O_3 particles play a major role in grain refinement. To further determine the influence of nano-Al_2O_3 particles and SiC_w on grain size, EBSD analysis was carried out, as shown in Figure 6. The movement of nano-Al_2O_3 particles on the grain boundary of the copper matrix produces Zener resistance, inhibits grain growth, and produces Hall-patch fine grain strengthening, according to the following equation [38]:

$$\sigma_{GR} = k(d_c^{-1/2} - d_m^{-1/2}) \tag{2}$$

where k is a constant (Cu = 0.07 MPa × $m^{0.5}$ [40]), d_c is the grain size of the SiC_w/Cu–Al_2O_3 composite (d_c = 1.43 μm), and d_m is the average size of pure Cu. The σ_{GR} value provided by nano-Al_2O_3 particles was calculated to be 35.6 MPa.

3.3.3 Load transfer

When the load is fully applied and the whiskers arranged along the tensile direction are evenly distributed in the copper matrix, load transfer strengthening can be effectively realized [41]. Whiskers or short fibers are pulled out and broken during stretching. When the length is less than a certain critical length will be drawn out. When the length of SiC_w is less than a certain critical length l_c, the whiskers or short fibers will be pulled out; otherwise, it will break. The critical length can be obtained according to the equilibrium condition of force [42]:

$$l_c = \frac{\sigma_{SiC_w}}{2\tau_y} D_{SiC_w};\ \tau_y \approx \frac{\sigma_{my}}{2} \tag{3}$$

where σ_{SiC_w} is the tensile strength (20.8 GPa) of SiC_w, D_{SiC_w} is the diameter of SiC_w (0.5 μm), τ_y is the matrix shear stress, and σ_{my} is the yield strength of the Cu matrix (200.1 MPa). According to the calculation, the critical length is 52 μm, which is far greater than the actual length of whiskers; so, SiC_w fails in the form of pulling out during the drawing process, which can be verified from Figure 5d. The strength increase provided by the load transfer strengthening of silicon carbide whiskers can be calculated by the following equation:

$$\sigma_{LT} = \left(\sigma_{SiC_w}\frac{l}{2l_c} - \sigma_{my}\right)f_{SiC_w} \quad (4)$$

where f_{SiC_w} is the volume of the reinforcing phase (4.7 vol%). According to equation (4), the contribution of load transfer enhancement to strength is 61.1 MPa. There is a positive correlation between the strength of the composites and the volume fraction of the reinforcing phase; that is, with increasing volume fraction, the strength of the composites increases gradually, but if the volume fraction of the reinforcing phase is too high, the strength of the composites will decrease.

3.3.4 Synergistic strengthening

The total contribution of various strengthening mechanisms in the $Cu–Al_2O_3$ composite is 370.9 MPa, which is 68.8 MPa less than the actual tensile yield strength (439.7 MPa). The total contribution of various strengthening mechanisms in the $SiC_w/Cu–Al_2O_3$ composite is 442 MPa, which is 33.9 MPa less than the actual tensile yield strength (475.9 MPa). Therefore, it can be inferred that the addition of SiC_w reduces the difference between the calculated and experimental values of single-reinforced composite ($Cu–Al_2O_3$) and double-reinforced composite ($SiC_w/Cu–Al_2O_3$), and nano-Al_2O_3 particles play a positive role in enhancing the load transfer of SiC_w. Liu *et al.* [43] studied the strengthening mechanism when SiC_w and nanoparticles were added alone or in combination and found that the combination of SiC_w and nanoparticles can change the microstructure of materials, and thus the mechanical properties of composites. Particle-whisker hybrid-reinforced copper matrix composites exert the advantages of each reinforced phase, and at the same time, each component synergistically strengthens copper matrix composites [37]. As seen in Figure 5c, agglomerated SiC_w can be seen in the fracture morphology of the SiC_w/Cu composite, but there is no large area of agglomerated SiC_w in the fracture morphology of the $SiC_w/Cu–Al_2O_3$ composite in Figure 5d.

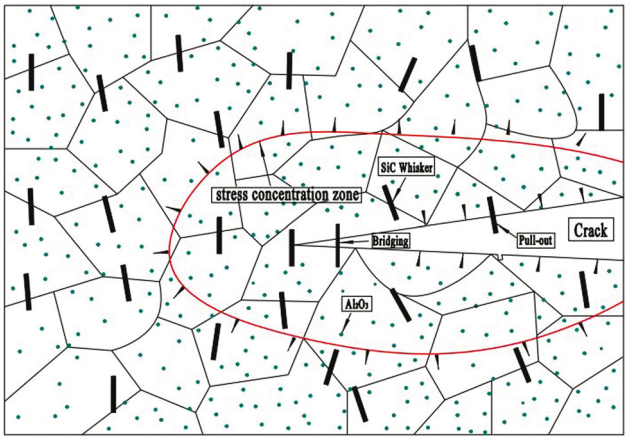

Figure 7: Schematic diagram of the particle and whisker hybrid-reinforced $SiC_w/Cu–Al_2O_3$ composite.

The synergistic effect is that nano-Al_2O_3 particles can adjust the spatial distribution of SiC_w in the copper matrix and reduce the agglomeration of SiC_w. With the addition of SiC_w, the distribution of nano-Al_2O_3 particles is more uniform, and the spatial configuration is better, as shown in Figure 7. The contact area between dispersed SiC_w and the copper matrix increases, which is beneficial for improving the interfacial bonding strength and reducing the shedding phenomenon caused by the agglomeration of SiC_w during stretching. Nano-Al_2O_3 particles further restrict the shedding and pulling-off of SiC_w and further improve the tensile strength of the $SiC_w/Cu–Al_2O_3$ composite. The above results show that SiC_w and nano-Al_2O_3 particles have synergistic effects on strengthening copper matrix composites. The difference between the calculated value and the experimental value can be regarded as the contribution value of thermal mismatch and synergistic strengthening mechanism to the strength of the $SiC_w/Cu–Al_2O_3$ composite, and the contribution ratio to the strength is 7.1%.

3.4 Arc erosion resistance of the $SiC_w/Cu–Al_2O_3$ composite

The distributions of arc duration and arc energy data of $Cu–Al_2O_3$ composite and $SiC_w/Cu–Al_2O_3$ composite are shown in Figure 8a and b. Arc duration and arc energy have the same fluctuation tendency. The electrical contact test of the $Cu–Al_2O_3$ composite cannot be continued after 1,500 operations due to the serious oxidation of the contact surface. The $SiC_w/Cu–Al_2O_3$ composite has good arc stability in the first 2,700 operation times, and the arc duration and arc energy increase sharply in the later

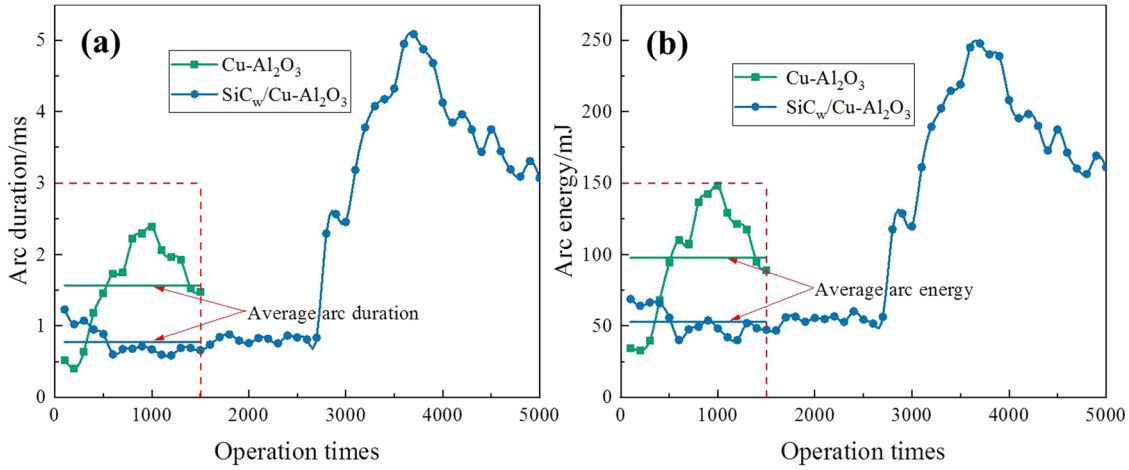

Figure 8: Fluctuation distribution curves of arc duration (a) and arc energy (b).

stage, but 5,000 operations have been successfully completed. Comparing the arc duration and arc energy of the first 1,500 operation times, it is found that the average arc duration and arc energy of the $SiC_w/Cu–Al_2O_3$ composite are lower than that of the $Cu–Al_2O_3$ composite, and the $SiC_w/Cu–Al_2O_3$ composite has a better arc stability. Therefore, the addition of SiC_w has a more significant effect on reducing the arc duration and energy of the $Cu–Al_2O_3$ composite.

Figure 9 shows the surface morphologies of anode and cathode contact materials after arc erosion. Compared with the erosion morphologies of the $SiC/Cu–Al_2O_3$ composite, the erosion area of the $Cu–Al_2O_3$ composite is larger. It is found that a large number of molten droplets adhere to the contact surface, which seriously damages the connectivity of the circuit and leads to the failure of the $Cu–Al_2O_3$ contact pairs. The electrical contact experiment shows that the arc erosion resistance of the

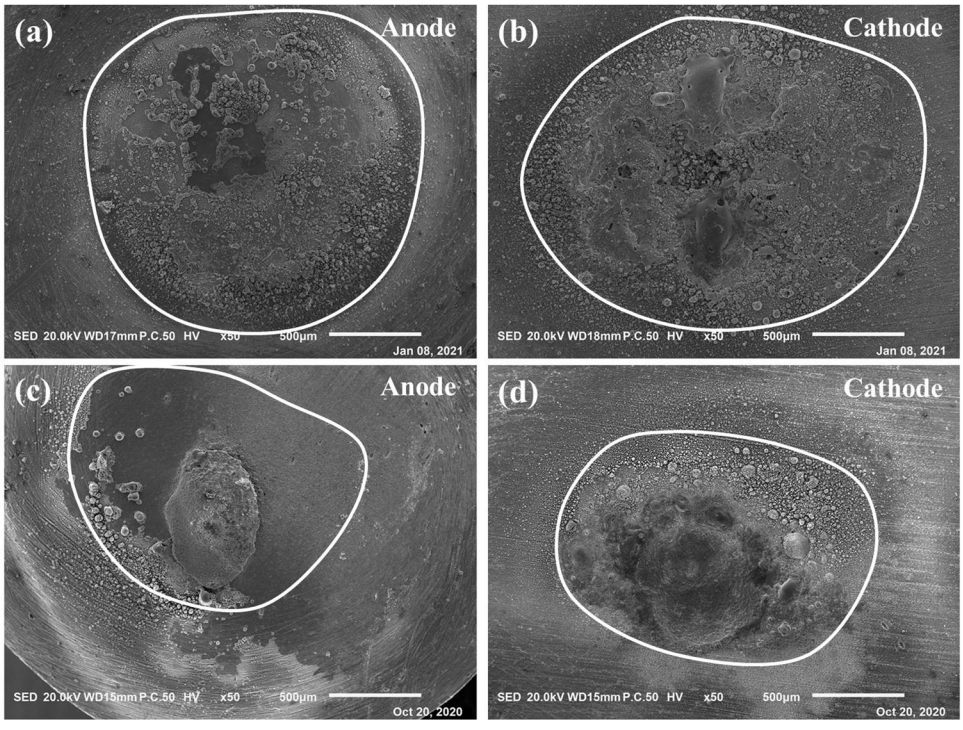

Figure 9: Erosion morphologies of anode and cathode for the $Cu–Al_2O_3$ composite (a and b) and the $SiC_w/Cu–Al_2O_3$ composite (c and d).

$Cu–Al_2O_3$ composite is far less than that of the SiC_w/$Cu–Al_2O_3$ composite.

4 Conclusions

(1) Nano-Al_2O_3 particles and SiC_w can adjust the spatial distribution of each other in the copper matrix, which is more conducive to fully exploiting the advantages of each reinforcing phase. The introduction of high-strength SiC_w can bridge the copper matrix, promote crack deflection, and further improve the tensile strength of copper matrix composites.
(2) Nano-Al_2O_3 particles and micro-SiC_w reinforcements synergistically strengthened the SiC_w/$Cu–Al_2O_3$ composite. Orowan strengthening is the main strengthening mechanism in the SiC_w/$Cu–Al_2O_3$ composite, accounting for 30.5%.
(3) The addition of SiC whiskers can improve the arc erosion resistance of the $Cu–Al_2O_3$ composite. Compared with the $Cu–Al_2O_3$ composite, the average arc duration and arc energy of the SiC_w/$Cu–Al_2O_3$ composite were lower, and the arc stability was better.

Funding information: This work was supported by the project of the National Natural Science Foundation of China (51605146, U1502274), Henan Provincial Key Young Teachers Training Program for Higher Education Institutions (2018GGJS045), China Postdoctoral Science Foundation (2020T130172, 2020M682288), Henan Province "Innovative Science and Technology Team" Program (182101510003), and the Key Scientific Research Projects of Higher Education Institutions in Henan Province (21A430014).

Author contributions: All authors have accepted responsibility for the entire content of this manuscript and approved its submission.

Conflict of interest: The authors state no conflict of interest.

References

[1] Feng J, Song KX, Liang SH, Guo XH, Jiang YH. Electrical wear of TiB_2 particle-reinforced Cu and Cu–Cr composites prepared by vacuum arc melting. Vacuum. 2020;175:92–5.
[2] Ma GZ, Xu BS, Wang HD, Wang XH, Zhang S. Research on the microstructure and space tribology properties of electric-brush plated Ni/MoS2-C composite coating. Surf Coat Technol. 2013;221:142–9.
[3] Shankar U, Naduvinamani NB, Basha H. A generalized perspective of fourier and fick's laws: magnetized effects of Cattaneo-Christov models on transient nanofluid flow between two parallel plates with brownian motion and thermophoresis. Nonlinear Eng. 2020;9(1):201–22.
[4] Jiang YH, Zhang XJ, Zhang XN, Lan T, Cao F, Liang SH. Structural heterogeneity and its effects on the properties of an in situ TiB_2–TiC/Cu composite synthesised by hot pressing. Powder Metall. 2020;63(2):126–33.
[5] Liang SH, Li WZ, Jiang YH, Cao F, Dong GZ, Xiao P. Microstructures and properties of hybrid copper matrix composites reinforced by TiB whiskers and TiB_2 particles. J Alloys Compd. 2019;797:589–94.
[6] Chen SH, Fu SL, Liang D, Chen XH, Mi XJ, Liu P, et al. Preparation and properties of 3D interconnected CNTs/Cu composites. Nanotechnol Rev. 2020;9(1):146–54.
[7] Zhu SX, Liu Y, Tian BH, Zhang Y, Song KX. Arc erosion behavior and mechanism of Cu/Cr_{20} electrical contact material. Vacuum. 2017;143:129–37.
[8] Afifeh M, Hosseinipour SJ, Jamaati R. Nanostructured copper matrix composite with extraordinary strength and high electrical conductivity produced by asymmetric cryorolling. Mater Sci Eng A. 2019;763:138146.
[9] Hwang SJ. The formation kinetics of Cr_2O_3 dispersed Cu synthesized by Cryo-milling. Rev Adv Mater Sci. 2020;59(1):47–53.
[10] Zhang YF, Ji Z, Jia CC, Liu GM, Wan FR, Zhan Q. Influence of lanthanum on enhancement of mechanical and electrical properties of $Cu–Al_2O_3$ composites. J Rare Earth. 2019;37(5):534–40.
[11] Pan Y, Xiao SQ, Lu X, Zhou C, Li Y, Liu ZW, et al. Fabrication, mechanical properties and electrical conductivity of Al_2O_3 reinforced Cu/CNTs composites. J Alloys Compd. 2019;782:1015–23.
[12] Singh MK, Gautam RK. Synthesis of copper metal matrix hybrid composites using stir casting technique and its mechanical, optical and electrical behaviours. Trans Indian Inst Met. 2017;70(9):2415–28.
[13] Dang C, Liu HM, Feng S, Qu Y, Hu QL, Jiang JC. Effect of La_2O_3 addition on copper matrix composites reinforced with Al_2O_3 ceramic particles. Mater Res Express. 2019;6(10):106312.
[14] Li SL, Guo XH, Zhang SL, Feng J, Song KX, Liang SH. Arc erosion behavior of TiB_2/Cu composites with single-scale and dual-scale TiB_2 particles. Nanotechnol Rev. 2019;8(1):619–27.
[15] Mani MK, Viola G, Reece MJ, Hall JP, Evans SL. Mechanical and magnetic characterisation of SiC whisker reinforced Fe-Co alloy composites. Mater Sci Eng A. 2014;592:19–27.
[16] Dong RH, Yang WS, Wu P, Hussain M, Wu GH, Jiang LT. High content SiC nanowires reinforced Al composite with high strength and plasticity. Mater Sci Eng A. 2015;630:8–12.
[17] Liu GM, Li B. Study on the electrical arc ablation performance of nano-SiC_w reinforced Cu-matrix composites. Adv Mat Res. 2011;228–9:509–13.
[18] Zhang WL, Ma X, Ding DY. Aging behavior and tensile response of a SiC_w reinforced eutectoid zinc-aluminium-copper alloy matrix composite. J Alloys Compd. 2017;727:375–81.

[19] Guo XH, Song KX, Liang SH, Wang X. Relationship between the MgOp/Cu interfacial bonding state and the arc erosion resistance of MgO/Cu composites. J Mater Res. 2017;32(19):3753–60.
[20] Song KX, Xing JD, Dong QM, Liu P, Tian BH, Cao XJ. Internal oxidation of dilute Cu–Al alloy powers with oxidant of Cu_2O. Mater Sci Eng A. 2004;380(1–2):117–22.
[21] Zhou DS, Geng HW, Zeng W, Zhang DL, Kong C, Munroe P. Suppressing Al_2O_3 nanoparticle coarsening and Cu nanograin growth of milled nanostructured Cu–5vol%Al_2O_3 composite powder particles by doping with Ti. J Mater Sci Technol. 2017;33(11):1323–8.
[22] An Z, Ohi A, Hirai M, Kusaka M, Iwami M. Study of the reaction at Cu/3C-SiC interface. Surf Sci. 2001;493(1):182–7.
[23] Zhang XN, Geng L, Wang GS. Fabrication of Al-based hybrid composites reinforced with SiC whiskers and SiC nanoparticles by squeeze casting. J Mater Process Tech. 2006;176(1–3):146–51.
[24] Pozuelo M, Kao WH, Yang JM. High-resolution TEM characterization of SiC nanowires as reinforcements in a nanocrystalline Mg-matrix. Mater Charact. 2013;77:81–8.
[25] Rajkovic V, Bozic D, Devecerski A, Jovanovic MT. Characteristic of copper matrix simultaneously reinforced with nano- and micro-sized Al_2O_3 particles. Mater Charact. 2012;67:129–37.
[26] Zhang XH, Xu L, Du SY, Han WB, Han JC, Liu CY. Thermal shock behavior of SiC-whisker-reinforced diboride ultrahigh-temperature ceramics. Scr Mater. 2008;59(1):55–8.
[27] Larionova T, Koltsova T, Fadin Y, Tolochko O. Friction and wear of copper-carbon nanofibers compact composites. Wear. 2014;319:118–22.
[28] Guo XH, Song KX, Liang SH, Wang X, Zhang YM. Effect of Al_2O_3 particle size on electrical wear performance of Al_2O_3/Cu composites. Tribol T. 2016;59(1):170–7.
[29] Guo XH, Song KX, Wang X, Li GH, Zhang ZL. Effect of TiB_2 particle size on the material transfer behaviour of Cu–TiB_2 composites. Mater Sci Technol. 2020;36(15):1685–94.
[30] Li M, Chen FY, Si XY, Wang J, Du SY, Huang Q. Copper-SiC whiskers composites with interface optimized by Ti_3SiC_2. J Mater Sci. 2018;53(13):9806–15.
[31] Ma K, Wen HM, Hu T, Topping TD, Isheim D, Seidman DN, et al. Mechanical behavior and strengthening mechanisms in ultrafine grain precipitation-strengthened aluminum alloy. Acta Mater. 2014;62:141–55.
[32] Cheng C, Song KX, Mi XJ, Wu BA, Xiao Z, Xie HF, et al. Microstructural evolution and properties of Cu–20 wt% Ag alloy wire by multi-pass continuous drawing. Nanotechnol Rev. 2020;9(1):1359–67.
[33] Rajkovic V, Bozic D, Stasic J, Wang HW, Jovanovic MT. Processing, characterization and properties of copper-based composites strengthened by low amount of alumina particles. Powder Technol. 2014;268:392–400.
[34] Chu K, Wang F, Li YB, Wang XH, Huang DJ, Zhang H. Interface structure and strengthening behavior of graphene/CuCr composites. Carbon. 2018;133:127–39.
[35] Wu Q, Miao WS, Zhang YD, Gao HJ, David H. Mechanical properties of nanomaterials: a review. Nanotechnol Rev. 2020;9(1):259–73.
[36] George R, Kashyap KT, Rahul R, Yamdagni S. Strengthening in carbon nanotube/aluminium (CNT/Al) composites. Scr Mater. 2005;53(10):1159–63.
[37] Long F, Guo XH, Song KX, Jia SG, Yakubovd V, Li SL, et al. Synergistic strengthening effect of carbon nanotubes (CNTs) and titanium diboride (TiB_2) microparticles on mechanical properties of copper matrix composites. J Mater Res Technol. 2020;9(4):7989–8000.
[38] Queyreau S, Monnet G, Devincre B. Orowan strengthening and forest hardening superposition examined by dislocation dynamics simulations. Acta Mater. 2010;58(17):5586–95.
[39] Wang XL, Wang YP, Su Y, Qu ZG. Synergetic strengthening effects on copper matrix induced by Al_2O_3 particle revealed from micro-scale mechanical deformation and microstructure evolutions. Ceram Int. 2019;45(12):14889–95.
[40] Chen XF, Tao JM, Yi JH, Liu YC, Li CJ, Bao R. Strengthening behavior of carbon nanotube-graphene hybrids in copper matrix composites. Mater Sci Eng A. 2018;718:427–36.
[41] Chen B, Li SF, Imai H, Jia L, Umeda J, Takahashi M, et al. Load transfer strengthening in carbon nanotubes reinforced metal matrix composites via in-situ tensile tests. Compos Sci Technol. 2015;113:1–8.
[42] Chen B, Shen J, Ye X, Imai H, Umeda J, Takahashi M, et al. Solid-state interfacial reaction and load transfer efficiency in carbon nanotubes (CNTs)-reinforced aluminum matrix composites. Carbon. 2017;114:198–208.
[43] Liu XF, Liu HL, Huang CZ, Wang LM, Zou B, Zhao B. Synergistically toughening effect of SiC whiskers and nanoparticles in Al_2O_3-based composite ceramic cutting tool material. Chin J Mech Eng. 2016;29(5):977–82.